Stabilizing Effect of Pseudo-Dendritic Polyethylenimine on Platinum Nanoparticles Supported on Carbon

Ping-Lin Kuo,*,† Wei-Fu Chen,† Hsin-Yeh Huang,† I-Chung Chang,† and Shenghong A. Dai‡

Department of Chemical Engineering, National Cheng Kung University, Tainan, Taiwan 70101, and Department of Chemical Engineering, National Chung Hsing University, Taichung, Taiwan 402

Received: October 5, 2005; In Final Form: January 4, 2006

A new type of surfactant with a hydrophile of dendritic polyethylenimine ($C_{12}(EI)_7$) was synthesized by a cationic polymerization of dodecylamine with aziridine and was used as a stabilizer to prepare Pt colloid, which is then used in situ to prepare carbon-supported Pt nanoparticles. The effects of supporting carbon, surfactant concentration, and calcination time on the nanoparticle size and catalytic performance were determined from the transmission electron microscopic analyses and cyclic voltammograms. In the presence of carbon, the Pt particle size increased slightly with lower $C_{12}(EI)_7$ content, while those with higher $C_{12}(EI)_7$ concentrations remained unchanged. For the heat-treated Pt/C catalyst, the molar ratio of $C_{12}(EI)_7$ to H_2PtCl_6 ([N]/[Pt] ratio) dominated the growth of Pt nanoparticles. The size decreased from 7.6 nm for a [N]/[Pt] ratio of 5 to 3.8 nm for a [N]/[Pt] ratio of 40. X-ray photoelectron spectroscopy revealed that metallic Pt^0 (81.6%) predominated the Pt species in the heat-treated catalyst, which is more than the commercial E-TEK catalyst. The data show clearly that thermal treatment had successively removed the stabilizing shells; moreover, it did not cause serious aggregation of particles in the presence of $C_{12}(EI)_7$ and thus enhanced the catalytic activity. The interaction between Pt and $C_{12}(EI)_7$ were studied and were explained in terms of a mechanism of dual-functional stabilization both on carbon and in the thermal treatment.

Introduction

Dendritic polymers with a well-defined structure, which have recently attracted significant interest, have been used as templates to host inorganic particles, as reported by many groups.[1−4] The stabilizing effect of these macromolecules is attributed to the fact that either the small particles or ions are attached to the much larger protecting polymers or molecules to cover or encapsulate the metal particles or ions. The preparation of nanoscopic metal particles is now of interest, because such particles have huge surface areas and possess unique properties that can be used in a wide range of applications. Of the most interest are nanocatalysts, which are crucial for use in fuel cells.[5] The state-of-the-art techniques for preparing carbon-supported catalysts still do not satisfy the requirements for use.[6−8] In the commercially used impregnation method, the microporosity of the carbon support would limit the accessibility of deposited platinum or ruthenium to the fuel (e.g., hydrogen or methanol). New synthetic strategies have been reported by many research groups to achieve well-dispersed Pt particles over the supporting carbon. They have employed various kinds of protecting agents such as ammonium salts, PVP, PVA, and so forth.[9−13] These protecting agents provide electrostatic repulsion or steric hindrance to preventing particle aggregation. The eletrocatalytic performance of these catalyst was found to be equivalent or slightly higher than that of the commercial E-TEK catalyst.

Recently, we have used pseudo-dendritic polymers such as pendant polyethyleniminated poly(allylamine) and ABA triblock polyethyleniminated poly(oxypropylene)diamines[14,15] as stabilizers to prepare several kinds of metal nanoparticles by the simple borohydride reduction method. In the present work, a novel difunctional polyethylenimine is synthesized through the polymerization of dodecylamine with aziridine, where the generated pseudo-dendritic polyethylenimine acts as the hydrophile. This polyethyleniminated dodecylamine ($C_{12}(EI)_7$) is used as a stabilizer to prepare Pt colloid, which is then used in situ to prepare carbon-supported Pt nanoparticles for the catalytic layer of fuel cells. The particles obtained in the colloid are small (about 3 nm), stable, and well-distributed, while those on the carbon surface after heat treatment depend on the surfactant content. This can be attributed to the protection from the dual-functional structure provided by the alkyl chains and the well-structured chelating hydrophiles, which also serve as a block to prevent Pt particles from depositing in the micropores. The effects of surfactant concentration, carbon support, and calcination time on the size and morphology of Pt nanoparticles have been characterized by transmission electron microscopy (TEM), X-ray diffraction (XRD), and X-ray photoelectron spectroscopy (XPS). The electrocatalytic performance of the Pt/C catalysts for methanol electro-oxidation has also been investigated by cyclic voltammetry (CV).

Experimental Section

Materials. Dodecacylamine ($C_{12}NH_2$) and ethanolamine were from Aldrich. Hexachloroplatinic acid ($H_2PtCl_6 \cdot 6H_2O$) was purchased from Alfa Aesor. Nafion solution (5 wt %) was from Du Pont, and carbon paper (Toray, 30 wt % wet-proofing) and commercial Pt catalysts (20 wt % loading) were provided by E-TEK Inc. Vulcan XC-72 used as catalyst support was obtained from Carbot (U.S.A.). Other chemicals including sodium peroxide (NaOH), sodium borohydride ($NaBH_4$), methanol

* To whom all correspondence should be addressed. Tel.: +886−6−275 7575−62658. Fax: +886−6−276 2331. E-mail: plkuo@mail.ncku.edu.tw.

† National Cheng Kung University.

‡ National Chung Hsing University.

10.1021/jp055688m CCC: $33.50
Published on Web 02/01/2006

SCHEME 1

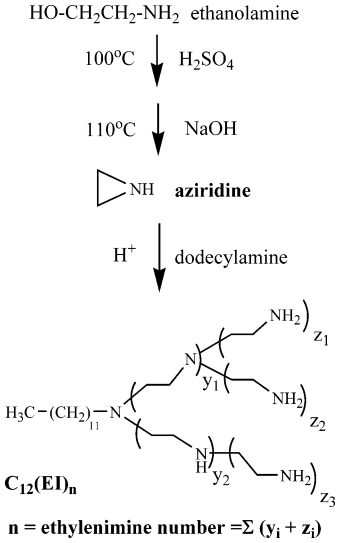

(CH_3OH), sulfuric acid (H_2SO_4), and isopropyl alcohol (IPA) were obtained from Aldrich. All materials were used as received without further purification from manufacturers. All aqueous solutions were prepared using deionized water purified through a Milli-Q system.

Syntheses of Polyethyleniminated Dodecane. The synthesis of polyethyleniminated dodecane ($C_{12}(EI)_n$) was based on a cationic polymerization method involving an acid-catalyzed reaction between aziridine and dodecylamine as shown in Scheme 1. A typical procedure for the reaction of dodecylamine with aziridine to produce $C_{12}(EI)_n$ is described as follows. The aziridine was freshly prepared according to the Wenker's method.[16] About 21.5 g (0.5 mol) of aziridine was mixed with 9.25 g (0.05 mol) of dodecylamine dissolved in 50 mL dichloromethane in the presence of a catalytic amount of acetic acid in a three-necked flask under N_2. The temperature was then increased to 80−85 °C and maintained for 20 h. After cooling to room temperature, the solvent was evaporated from the final solution. For purification, the crude product was dissolved in water and extracted repeatedly with chloroform to remove the un-alkylated polyethylenimine. After extraction, the chloroform was removed by a rotary evaporator, and the product was dried under vacuum for 48 h at a temperature of 60 °C. A slightly yellowish viscous liquid product was obtained with a yield of 67%. The average number of ethylenimine groups on the surfactant (n) was determined to be 7.1 by ^{1}H NMR. [N] is defined as the total normality concentration of amino groups on $C_{12}(EI)_7$.

^{1}H NMR (D_2O, ppm): δ 0.85 (−C*H*$_3$), δ 1.23 (−C*H*$_2$−), 1.45 (−CH$_2$−C*H*$_2$−N−), 2.3−3.0 (−N−C*H*$_2$−C*H*$_2$−N−), 3.3−3.5 (hydrogen on methylene carbon attached to the quartery amine). ^{13}C NMR (D_2O, ppm): δ 14.0 (−*C*H$_3$), 23.0 (−C*H*$_2$−CH$_3$), 27.0−30.5 (carbon on the alkyl chain), 32.0 (−C*H*$_2$−CH$_2$−CH$_3$), 37.8−41.0 (methylene carbon attached with the terminal amine), 44.0−56.0 (−N−*C*H$_2$−*C*H$_2$−N− and −CH$_2$−CH$_2$−*C*H$_2$−N−). IR (liquid film, cm^{-1}): 3500−3250, 2924, 2852, 1652, 1467, 1361, 1301, 1120−1050.

Syntheses of Pt Nanocatalyst. Typically, 100 mL of 0.5 mM [N] of $C_{12}(EI)_7$ and 0.1 mM H_2PtCl_6 aqueous solution was prepared. Because the Pt precursor (H_2PtCl_6) is very acidic, the addition of H_2PtCl_6 into $C_{12}(EI)_7$ solution decreased the pH value to around 4−6, resulting in a protonation toward most amino groups which decreases the strength of the coordination bonding between Pt(IV) and amino groups. The pH value was adjusted around 9.2 by a 0.1 N of NaOH aqueous solution, which can promote the ligand exchange between $PtCl_6^{2-}$ and the amino groups on $C_{12}(EI)_7$ to ensure that all the Pt ions are complexed with $C_{12}(EI)_7$. A 5×10^{-4} mol of sodium borohydride was then added at room temperature with vigorous stirring. Finally, brown transparent solutions of platinum colloids were obtained.

The Pt/C catalysts were prepared by combining Pt colloidal solutions with a suspension of Vulcan XC-72 (S_{BET} = 236.8 m^2 g^{-1})[17] in water and were stirred vigorously for 1 h. A nominal metal content of 20 wt % was taken on all the catalysts. The obtained Pt/C colloidal solution does not precipitate within 2 days and thus is considered a well-dispersed aqueous suspension. Then, the centrifugation process was performed to separate the solid residue and solvent at a speed of 5000 rpm for 30 min. The resulting solids were washed with a copious amount of distilled water to remove excess Cl^- and finally dried in an oven at 90 °C. Heat treatment was performed in nitrogen atmosphere at 280 °C. The catalysts were calcined for 5 and 10 h and then ground slightly in agate mortar. The resulting powder was used to prepare working electrodes.

The working electrode is a thin layer of Nafion-impregnated catalyst cast on a vitreous carbon disk with 1 cm^2 surface area. The Pt loading of the working electrode was fixed at 1 mg cm^{-2}. The catalyst powder was dispersed in 2-propanol and stirred vigorously for 1 h. Then, 2.5 wt % Nafion solution was added into the slurry by keeping the ratio of catalyst to Nafion (dry) at 1:3. After ultrasonication for 1 h, the resulting ink was spread on a carbon disk and dried under vacuum at 60 °C for 3 h.

Characterizations. The morphology, size, and size distribution of these catalysts were characterized by transmission electron microscopy (TEM) using a JEOL JEM-1200CX microscope operating at 120 kV. Specimens were prepared by placing a drop of the colloidal dispersion onto 200-mesh copper grids coated with an amorphous Formvar carbon film and dried overnight at room temperature in a vacuum oven before introducing the grid into the microscope.

TG analysis was performed on a thermogravimetric analyzer (Perkin-Elmer TGA 7) over a temperature range of 50−500 °C at a heating rate of 20 °C/min under nitrogen atmosphere. X-ray powder diffraction (XRD) was performed on a Rigaku RINT2100 X-ray diffractometer with Cu Kα radiation (λ = 0.1524 nm) operated at 40 kV and 40 mA by placing the powder of carbon-supported catalysts onto a glass slide. X-ray photoelectron spectroscopy (XPS) measurements were carried out with a VG Scientific ESCALAB 210 electron spectrometer using Mg Kα radiation under a vacuum of 2×10^{-8} Pa. Narrow scan photoelectron spectra were recorded for the C 1s, O 1s, N 1s, and Pt 4f regions and analyzed by deconvolution to estimate the surface oxidation states of the catalysts.

A CHI-608A potentiostat/galvanostat and a conventional three-electrode test cell were used for electrochemical measurements. Pt wire and Ag/AgCl electrode were used as the counter and reference electrodes, respectively. All electrolyte solutions were degassed by purging N_2 for 3 h prior to every measurement. The cyclic voltammetry (CV) experiments were performed in a 1 M H_2SO_4/2 M CH_3OH solution at 40 °C. Stable voltammograms recorded after at least 20 cycles were taken into account for data interpretation.

Results and Discussion

Synthesis of Pseudo-Dendritic Polyethyleniminated Dodecane. The synthesis of hyperbranched polyethylenimine derived from the exhaustive alkylation of the terminal amino group of dodecylamine with activated aziridine to produce a dendron-

TABLE 1: Characteristic Data for Hyperbranched Polyethyleniminated Dodecylamine Surfactant

EI number[a]		7.1
total amine values (mol/g)	nominal value	0.0165
	exptl value[b]	0.0163
amine (%)	primary	61.2
	secondary	14.2
	tertiary	24.6
T_d (°C)[c]		281

[a] The average ethylenimine groups determined by H^1 NMR spectrum. [b] The amine values were measured by potential titration analysis. [c] The onset temperature of maximum decomposition rate.

like structure is shown in Scheme 1. Higher generations were obtained by simply adding supplementary aziridines. The possibilities of defect become progressively greater, and the branching becomes more complex owing to the divergence growth, resulting in a mixture of primary, secondary, and tertiary amines. The polyethyleniminated alkylamine is a new dendron-like surfactant expressed as $C_{12}EI_n$ according to their ethylenimine numbers (EI, n). The length of the polyethylenimine chain attached on the terminal amino group was determined from the ^1H NMR spectra of the obtained surfactants. From the ratio of the area integral of the terminal methyl protons and EI protons, the average EI number was quantitatively calculated to be $n = 7.1$ (Supporting Information Figure S1a).

The FT-IR spectrum of the surfactant $C_{12}(EI)_7$ displays the characteristic absorption peak due to amine stretching vibrations around 3500−3250 cm^{-1}. The relative intensities between this peak and the C−H vibrations at 2924 and 2852 cm^{-1} increase significantly after the ethylenimines attach onto the dodcylamine (Figure S1b). The total amine value obtained by potentiometric titration shows that the experimental value of 0.0163 mol/g is very close to the nominal one (0.0165 mol/g). We also determined quantitatively the average percentage of those amines in $C_{12}(EI)_7$ by potentiometric titration, and the results revealed that it contains 61.2, 14.2, and 24.6% of primary, secondary, and tertiary amines, respectively, as shown in Table 1. This indicates that $C_{12}(EI)_7$ has a dendritic structure with a very high degree of branching.

Stabilizing Effect of $C_{12}EI_7$ on Formation of Pt and Pt/C Colloids. Metal colloids passivated by amino-containing dendrimers[18] or pseudo-dendritic polymers[4,19] that have been synthesized by several research groups evidenced the strong complexation between amino groups and metal atoms. Stabilization of the Pt particles by $C_{12}(EI)_7$ can be discussed mainly from the viewpoint of complexing ability and steric effect. On one hand, the dendritic-structured amino groups on $C_{12}(EI)_7$ can be considered a highly effective chelating agent to metal ions or atoms, and on the other hand, $C_{12}(EI)_7$ possesses excellent surface active properties because of its intrinsically amphiphilic nature resulting from the lipophilic alkyl chain and the hydrophilic amino segment. The dodecyl chain surrounding the complexed metal core inhibits the particles from undergoing any kind of agglomeration. The coverage of the metal particles by the alkyl groups exerts remarkable stability on the particles. It is worth mentioning that Manna et al. made an extensive investigation on the stabilization mechanism in their synthesis of stable silver nanoparticles using the surfactant *N*-hexadodecylethylenediamine with the reducing agent $NaBH_4$ by a two-phase redox reaction carried out in a heptane/water system. They explained that the formation of alkyl chain bilayer on the surface of nanoparticles provides a stabilizing effect for nanoparticles from aggregation. In the present investigation, the dodecyl chain and dendritic-structured amino groups can further attach onto the carbon surface through van der Waals interaction and static attraction, respectively.

TABLE 2: Average Particle Sizes and Standard Deviations of the Pt or Pt/C Colloids

[N]/[Pt]	d_b (nm)[a]	d_c (nm)[b]	t (h)[c]	d_{XRD} (nm)[d]	d_{TEM} (nm)[e]
5	3.5 ± 1/1	5.0 ± 1.6	5	9.8	7.6 ± 2.1
10	3.1 ± 0.8	3.1 ± 0.7	5	6.3	6.2 ± 1.2
20	2.9 ± 0.9	2.9 ± 0.7	0		
20			5	3.7	4.1 ± 1.0
20			10	4.1	4.5 ± 1.0
40	2.6 ± 0.6	2.5 ± 0.6	5	3.7	3.8 ± 0.8

[a] Mean particle sizes of the unsupported Pt nanoparticles. [b] Mean particle sizes of the Pt/C catalyst before heat treatment. [c] The time of heat treatment. [d] Grain sizes calculated by XRD after heat treatment. [e] Particle sizes determined by TEM after heat treatment.

The preparation of Pt and Pt/C colloids was based on a modified approach reported by Liu et al.[20] The TEM images of Pt colloids (see Figure S2) show remarkably uniform and highly dispersed metal particles. The average diameters (d_b) ranging from 2.6 to 3.5 nm are obtained as shown in Table 2. With increasing [N]/[Pt] ratios, the particle sizes and their standard deviations decrease slightly. This is probably because, with a higher molar ratio of $C_{12}(EI)_7$/Pt, a strong coordination affinity of the surfactant with $PtCl_6^{2-}$ ions could be realized, thereby causing a decrease in the surface energy of Pt particles after subsequent reduction by $NaBH_4$. On the other hand, the strong hydrophobic interaction of $C_{12}(EI)_7$ with the Pt particles prevents agglomeration of the metal particles. Adsorption of the metal colloids on Vulcan XC-72 carbon brings about some morphological changes (Figure S3). Of the four [N]/[Pt] ratios of 5, 10, 20, and 40, the stabilization effect is more pronounced at the ratio of 10 (3.1 ± 0.7 nm), which in turn leads to the formation of small particle size with uniform size distribution (denoted as d_c). Comparing the sizes and the size distributions with a [N]/[Pt] ratio of 5 in Table 2 shows that the colloids become larger and widely distributed after being adsorbed on carbon (from 3.5 ± 1.1 nm to 5.0 ± 1.6 nm). When the concentration of $C_{12}(EI)_7$ increases, the Pt nanoparticles are in a state of high dispersion over the carbon surface, and the sizes of the particles remain almost unchanged after being adsorbed on carbon. It should be noted that all the Pt nanoparticles of each sample deposited on the supporting carbon. This can be attributed to two reasons. One is the hydrophobic and/or van der Waals interaction between the alkyl chain of $C_{12}(EI)_7$ and the carbon surface. Another results from the static attraction force between the dendritic structured amino groups of $C_{12}(EI)_7$ and the carboxylic groups on carbon. The Pt nanoparticles are drawn simultaneously with the $C_{12}(EI)_7$ molecules attached onto the surface of carbon. Thus, it is proposed that the presence of $C_{12}(EI)_7$ surfactant can not only stabilize the unsupported Pt nanoparticles by its well-structured amino groups, but can also stabilize the carbon-supported ones by its dual-functional stabilizing mechanism provided by the alkyl chain and amino groups.

Thermal treatment of $C_{12}(EI)_7$-stabilized Pt/C catalysts was carried out at 280 °C (the thermal decomposition temperature was determined by the thermogram of $C_{12}(EI)_7$ in Figure S4a to be about 281 °C) under nitrogen to remove the stabilizing $C_{12}(EI)_7$ layer (Figure S4b). The weight loss of the $C_{12}EI_7$-stabilized Pt/C colloids with a [N]/[Pt] ratio of 20 during the thermal treatment reached a steady value at about 300 min. The remaining weight percent of 80.1% is close to the theoretical value of 80.3%, indicating a complete removal of the stabilizing layer. Adsorption of the colloidal particles on carbon followed

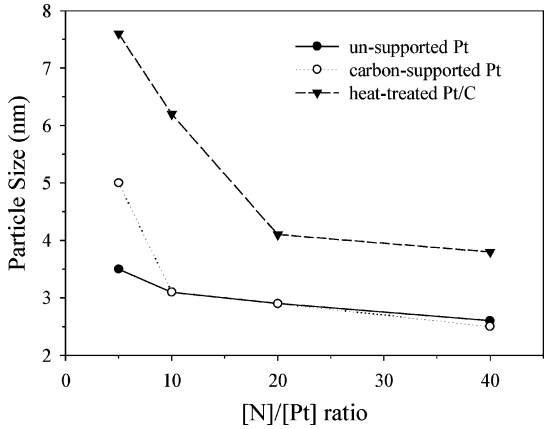

Figure 1. The relationship between particle sizes and [N]/[Pt] ratios of Pt particles and Pt/C colloids before and after thermal treatment.

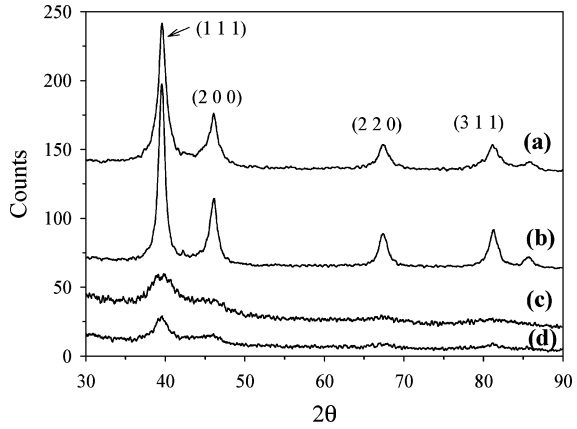

Figure 2. X-ray diffraction patterns of the Pt/C catalysts after thermal treatment at 280 °C for 5 h with [N]/[Pt] ratios of (a) 5, (b) 10, (c) 20, and (d) 40.

by thermal treatment at 280 °C for 5 h under N_2 did not bring about significant morphological changes with the [N]/[Pt] ratios of 20 and 40 (d_{TEM} in Table 2, 4.1 ± 1.0 and 3.8 ± 0.8 nm, respectively). For lower [N]/[Pt] ratios of 5 and 10, severe coalescence of the particles takes place leading to an enlargement of particle sizes. Both the mean diameters and the standard deviations of particles decrease significantly with increasing [N]/[Pt] ratios. The dependence of the mean diameters of unsupported Pt particles and Pt/C colloids before and after thermal treatment on [N]/[Pt] ratios is plotted in Figure 1. It can be clearly seen that, although the sizes of all cases increase after thermal treatment, with a sufficient amount of $C_{12}(EI)_7$ the aggregation of Pt particles is limited. We proposed that the steric effect of the alkyl chain should provide a good protective effect against the growth of particles, especially at a [N]/[Pt] ratio higher than 20, favoring the formation of small particles with a high uniformity.

The powder XRD patterns of the heat-treated Pt/C catalysts with [N]/[Pt] ratios of 5, 10, 20, and 40 are shown in Figure 2. All the catalysts exhibit the characteristic diffraction peaks at 2θ of 39°, 46°, 67°, 81°, and 86°, which are designated as Pt {111}, {200}, {220}, {311}, and {222} facets of the fcc crystal structure, respectively.[21] The lattice constant calculated from the {111} peak of the sample with a [N]/[Pt] ratio of 5 is 3.92 Å and is consistent with that of the bulk Pt {111} plane, i.e., 3.923 Å. The bandwidths become slightly broader for higher [N]/[Pt] ratios, while the lattice constant remains unchanged. The particle sizes (d_{XRD}) were obtained by measuring the broadening of the {111} peaks and applying the Scherrer

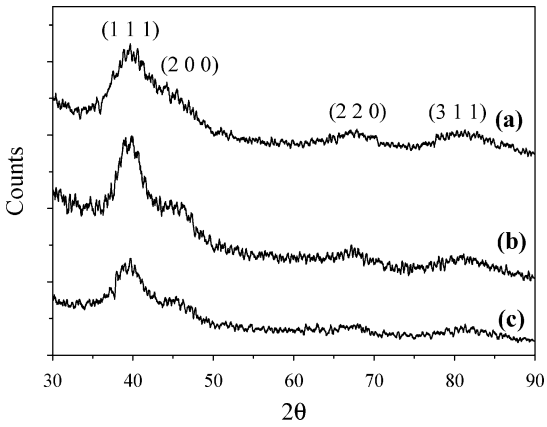

Figure 3. X-ray diffraction patterns of the Pt/C catalyst ([N]/[Pt] ratio = 20) with different heat-treated time: (a) without heat treatment, (b) 5 h, and (c) 10 h.

equation.[22] The calculated sizes of the samples with a [N]/[Pt] ratio of 5, 10, 20, and 40 are 9.8, 6.3, 3.7, and 3.7 nm, respectively, which are parallel to those obtained by TEM.

According to the above results, the aggregation of particles during thermal treatment is suppressed by increasing the surfactant content. It is of interest to examine the change in the particles when being heat-treated for a longer time. The mean particle size of the Pt/C catalyst with [N]/[Pt] of 20 after being heat-treated for 10 h (Figure S6) does not increase much (4.5 nm). This may be due to the existence of some residues or chars on the surface of Pt nanoparticles, which immobilize these particles and prevent them from being fused together. The powder XRD patterns of the Pt/C ([N]/[Pt] = 20) catalysts with different heat treatment times of 0, 5, and 10 h at 280 °C are displayed in Figure 3. The Pt {111} peaks become sharper and more intense with longer heat treatment , suggesting a greater enhancement in the degree of crystallization attributed to the thermal effect. Thermal treatment induces a growth of Pt nanoparticles from 2.9 to 4.5 nm when the calcination time increases to 10 h. In summary, the thermal treatment not only removes $C_{12}(EI)_7$, but also improves the crystallinity of Pt/C catalysts. Although their sizes are increased as well, the consequent average diameters are still quite satisfactory for the application in catalysts of fuel cells.

XPS Analysis of Pt/C Catalysts. The interactions between $C_{12}(EI)_7$ and Pt nanoparticles as well as their surface elemental compositions have been investigated by the XPS measurements. The survey scan of XPS of the Pt/C catalyst after thermal treatment at 280 °C under N_2 for 5 h is shown in Figure 4a. No signal in the Cl 2p region at about 200 eV is found indicating that chlorine has been removed in the preparation process. The regional N 1s spectra of the Pt/C catalyst (N/Pt = 20) before and after heat treatment at 280 °C under N_2 for 5 h are given in Figure 4b. The N 1s line is deconvoluted into three components at 398.0, 399.2, and 400.4 eV. The first peak at 398.0 eV is assigned to a nitride, indicating the presence of a metal−nitrogen bond.[23,24] The second one at 399.2 eV can be attributed to the H-bonded amine groups,[25,26] and the third one at 400.4 eV suggests the presence of N as protonated species such as quaternary ammonium ions (NR_4^+).[27] As shown in the inset of Figure 4b, the spectral regions of N 1s bands of Pt/C catalyst after heat treatment at 280 °C for 5 h show no visible peak of the N 1s signal, suggesting an almost complete removal of the $C_{12}EI_7$ molecules from the catalyst surface. These results are in full agreement with those of TG analysis and demonstrate clearly the effective removal of a stabilizing shell under the calcination condition to a level at least below the detection limit.

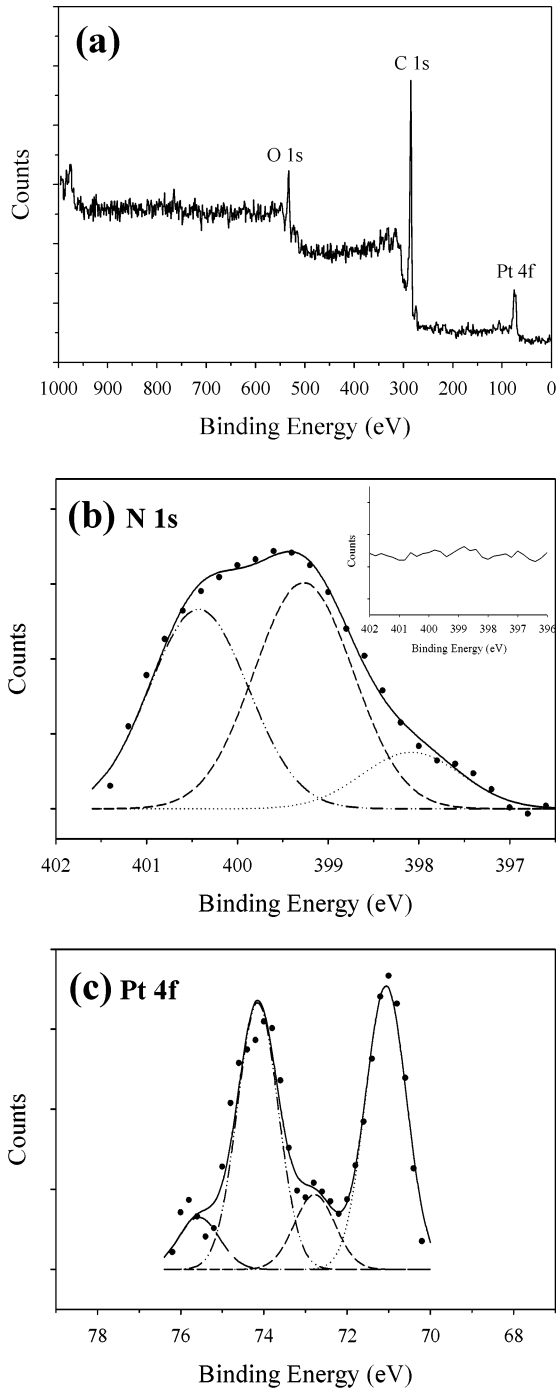

Figure 4. The XPS spectra of the Pt/C catalyst: (a) the survey scan after thermal treatment; (b) N 1s region before and after (the inset) thermal treatment; (c) Pt 4f region after thermal treatment. All the heat-treated samples are calcinated at 280 °C under N_2 for 5h.

In Figure 4c, the Pt 4f line of the heat-treated Pt/C catalyst shows two pairs of doublets from the spin−orbital splitting of the $4f_{7/2}$ and $4f_{5/2}$. The most intense doublets observed at 71.0 and 74.2 eV are attributed to zero valent platinum (Pt^0). The binding energies of the components along with the relative intensity for these samples are displayed in Table 3. The second set of doublets obtained at 72.8 and 75.6 eV can be ascribed to Pt(II) chemical states, such as PtO and $Pt(OH)_2$ species,[28,29] indicating the presence of Pt oxides. The existence of the Pt(II) state is well-known, because fine Pt particles are always covered with the chemisorbed oxygen.[30] The percentage of each component is obtained from the relative areas of these peaks. As shown in Table 3, the percentage of Pt^0 is 81.6% in the Pt/C catalysts, much higher than 73.64% of the E-TEK Pt/C catalyst.[31] The results reveal that the metallic Pt^0 is the predominant species in Pt/C catalysts. Catalysts with surface platinum of metallic state provide active sites for hydrogen or methanol oxidation rather than the Pt(II) species. Therefore, the major amount of metallic Pt^0 for Pt-based catalysts is required for high electrocatalytic activity.

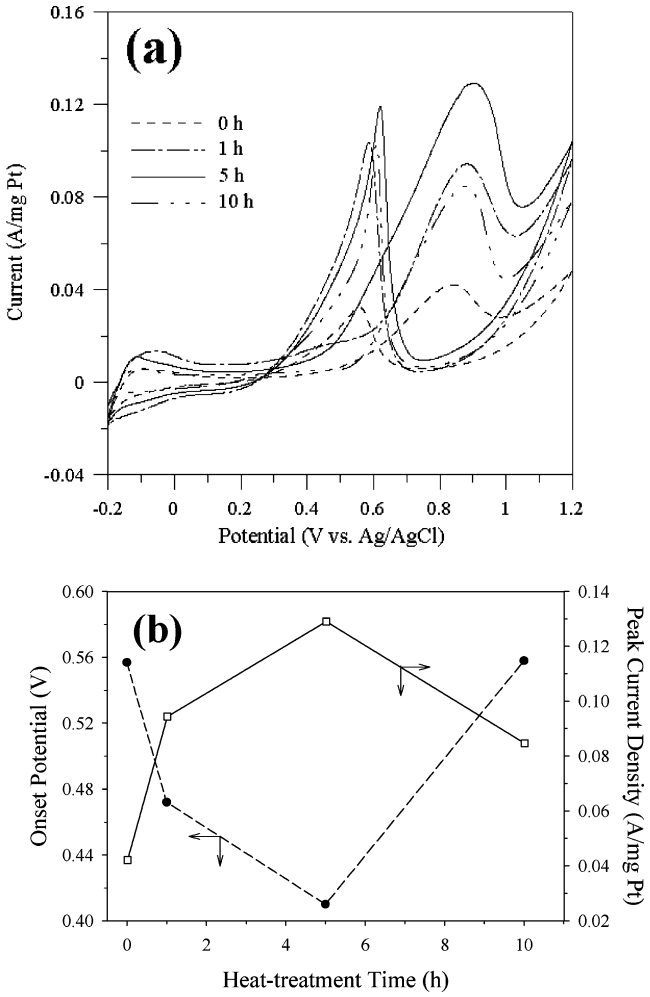

Figure 5. (a) Cyclic voltammograms of the Pt/C catalysts after heat treatment of 0, 1, 5, and 10 h in 1 M H_2SO_4/2 M CH_3OH solution with [N]/[Pt] = 20. (b) The onset potentials and peak current densities as a function of heat treatment time.

TABLE 3: Binding Energy and Relative Intensities of Different Species from Curve-Fitted X-ray Photoelectron Spectra in the N1s Region of the As-Prepared Pt/C Catalyst ([N]/[Pt) = 20) and in the Pt 4f Region of Heat-Treated Pt/C Catalyst at 280 °C under N_2 for 5h

species	binding energies (eV)		relative intensity (%)
N 1s	398.0		11.8
	399.2		47.2
	400.4		41.0
Pt 4f	71.0	74.2 (Pt^0)	81.6
	72.8	75.6 (Pt(II) species)	18.4

Performance in Methanol Electro-Oxidation. The as-prepared and heat-treated Pt/C catalysts ([N]/[Pt] = 20) with different heat treatment duration were characterized by cyclic voltammetry (−0.2 to 1.0 V, 20 mV s^{-1}) for methanol electro-oxidation in 1 M H_2SO_4/2 M CH_3OH solutions. For all Pt/C catalysts, pronounced features appear in both the anodic and cathodic sweeps as shown in Figure 5a. The peaks at around 0.85 V in the forward scan are attributed to the electro-oxidation of methanol. As can be seen in Figure 5b, the current density

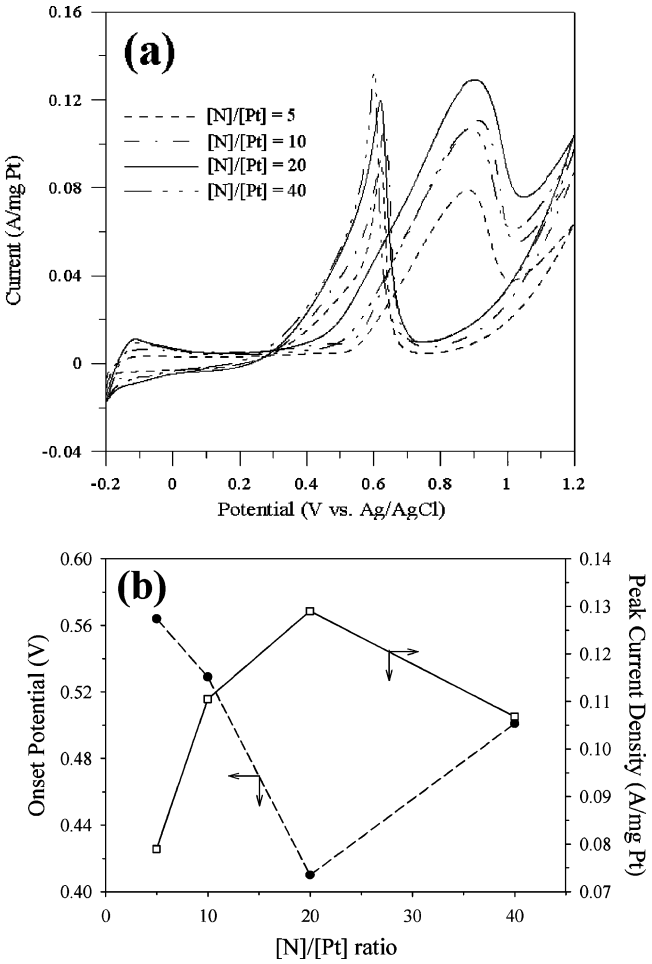

Figure 6. (a) Cyclic voltammograms of the heat-treated Pt/C catalysts at 280 °C with [N]/[Pt] = 5, 10, 20, and 40 in 1 M H_2SO_4/2 M CH_3-OH solution. (b) The onset potentials and peak current densities as a function of [N]/[Pt] ratios.

of this anodic peak increases with the heat-treated duration and reaches a maximum at 5 h, indicating that maximum improvement in catalytic activity can be achieved by balancing the extent of decomposition of $C_{12}(EI)_7$ and the increase in particle sizes during thermal treatment. The anodic peaks at around 0.56 V in the reverse scan are generally accepted as the removal of the incompletely oxidized carbonaceous species formed in the forward scan.[32,33] These carbonaceous species are mostly in the form of linearly bonded Pt═C═O, which causes the poisoning of Pt catalysts.

The cyclic voltammograms of the Pt/C catalysts with different [N]/[Pt] ratios in 1 M CH_3OH/0.5 M H_2SO_4 are given in Figure 6a. The characteristic CV parameters of the different electrodes obtained from these curves are plotted versus the [N]/[Pt] ratios as shown in Figure 6b. The onset potential decreases from 0.56 to 0.41 V, while the peak current density increases from 0.079 to 0.129 A/mg Pt with increasing [N]/[Pt] molar ratio to 20, demonstrating that the Pt/C catalysts with higher [N]/[Pt] ratios possess better activity for methanol oxidation. Since the difference in particle sizes between Pt/C catalysts with [N]/[Pt] ratios of 20 and 40 (4.1 and 3.8 nm, respectively) are small enough to be neglected, the decay at [N]/[Pt] ratio of 40 (from 0.129 to 0.107 A/mg Pt) does imply the presence of residual $C_{12}(EI)_7$ in the aftermath of incomplete decomposition under this calcination condition. In summary, two conclusions can be drawn from the above results: First, the increasing peak current density below [N]/[Pt] ratio of 20 should be ascribed to the decreasing particle size and narrow size distribution of Pt nanoparticles. Second, excess $C_{12}(EI)_7$ beyond the [N]/[Pt] ratio of 20 poses a problem to the calcination process.

From the above results of CV and TEM, it can be concluded that the activity of the Pt/C catalyst toward methanol oxidation is dominated by particle size. It has been well-known that Pt catalysts activate the C−H bonds of methanol in the electro-oxidative catalysis, resulting in the formation of Pt−CO surface species, that is, the CO poisoning of the anode catalysts. For further oxidation of CO to CO_2, according to the observations of Frelink et al.,[34,35] the formation of an adsorbed hydroxy species must be required. Accordingly, in the present study, the dependence of the activity of Pt catalysts on particle size can be derived in terms of either the increasing amount of Pt−OH species or the raised number of methanol adsorption sites. From the practical point of view, carbon-supported Pt nanoparticles provide excellent electrochemically active surface areas, and the function in producing Pt−OH species is very important for the application of fuel cells as catalyst layers.

Conclusion

A hyperbranched surfactant, polyethleniminated dodecane ($C_{12}(EI)_7$), was successfully prepared, and the synthesis of Pt nanoparticles supported on Vulcan XC-72 has been achieved through the reduction by sodium borohydride using $C_{12}(EI)_7$ as the stabilizer. The average size of the Pt nanoparticles decreases with increasing [N]/[Pt] ratios, reaching a plateau at a [N]/[Pt] ratio of 10. After thermal treatment, aggregation of the particles occurs at a [N]/[Pt] ratio of 5, leading to the enlargement of the mean diameter from 5.0 to 7.6 nm. In particular, for the [N]/[Pt] ratio of 20, the growth in particle size is restricted even with a heat treatment time of 10 h (from 2.9 to 4.5 nm), indicating an optimum value of the [N]/[Pt] ratio for the heat treatment process. All catalysts are characterized by fcc phase in XRD analysis, and the dimensions of nanocrystals calculated from diffraction peak widths are consistent with the TEM results. After heat treatment, the catalysts have primary improvements in their crystallinity rather than the growth in particle size. A significant amount of Pt in the metallic state is observed by XPS measurements (81.6%), with these values being higher than those of the commercial E-TEK catalyst (73.64%). The spectrum of the N 1s region has proved the interaction between $C_{12}EI_7$ and Pt particles on the catalyst surface before thermal treatment. The electrocatalytic activity of Pt/C catalysts ([N]/[Pt] = 20) was enhanced by thermal treatment. The peak current densities reached a maximum at heat treatment time of 5 h, demonstrating an optimum condition for the elimination of surfactants and the agglomeration of particles.

Acknowledgment. We gratefully acknowledge the National Science Council, Taipei, Taiwan for their generous financial support of this research.

Supporting Information Available: Supplemental figures regarding the NMR and FT-IR spectra (Figure S1), TEM images (Figure S2, S3, S5, and S6), as well as the TGA thermogram (Figure S4). This material is available free of charge via the Internet at http://pubs.acs.org.

References and Notes

(1) Balogh, L.; Tomalia, D. A. *J. Am. Chem. Soc.* **1998**, *120*, 7355.
(2) Crooks, R. M.; Zhao, M.; Sun, L.; Chechik, V.; Yeung, L. K. *Acc. Chem. Res.* **2001**, 34, *3*, 181.
(3) Esumi, K.; Suzuki, A.; Aihara, N.; Usui, K.; Torigoe, K. *Langmuir* **1998**, *14*, 3157.
(4) Kuo, P. L.; Chen, W. F. *J. Phys. Chem. B* **2003**, *107*, 11267.

(5) Carrette, L.; Friedrich, K. A.; Stimming, U. *ChemPhysChem* **2000**, *1*, 162.
(6) Chan, K. Y.; Ding, J.; Ren, J.; Cheng, S.; Tsang, K. Y. *J. Mater. Chem.* **2004**, *14*, 505.
(7) Wasmus, S.; Küver, A. *J. Electroanal. Chem.* **1999**, *461*, 14.
(8) Lamy, C.; Lima, A.; LeRhun, V.; Delime, F.; Coutanceau, C.; Léger, J. M. *J. Power Sources* **2002**, *105*, 283.
(9) Prabhuram, J.; Wang, X.; Hui, C. L.; Hsing, I. M. *J. Phys. Chem. B* **2003**, *107*, 11057.
(10) Kim, T.; Takahashi, M.; Nagai, M.; Kobayashi, K. *Electrochim. Acta* **2004**, *50*, 817.
(11) Wang, X.; Hsing, I. M. *Electrochim. Acta* **2002**, *47*, 2981.
(12) Liu, Z.; Ling, X. Y.; Lee, J. Y.; Su, X.; Gan, L. M. *J. Mater. Chem.* **2003**, *13*, 3049.
(13) Bönnemann, H.; Richards, R. M. *Eur. J. Inorg. Chem.* **2001**, 2455.
(14) Kuo, P. L.; Ghosh, S. K.; Liang, W. J.; Hsieh, Y. T. *J. Polym. Sci., Part A: Polym. Chem.* **2001**, *39* (17), 3018.
(15) Kuo, P. L.; Liang, W. J.; Wang, F. Y. *J. Polym. Sci. Part A: Polym. Chem.* **2003**, *41*, 1360.
(16) Wenker, H. *J. Am. Chem. Soc.* **1935**, *57*, 2328.
(17) Zhou, Z.; Wang, S.; Zhou, W.; Jiang, L.; Wang, G.; Sun, G.; Zhou, B.; Xin, Q. *Phys. Chem. Chem. Phys.* **2003**, *5*, 5485.
(18) Manna, A.; Imae, T.; Aoi, K.; Okada, M.; Yogo, T. *Chem. Mater.* **2001**, *13*, 1674.
(19) Kuo, P. L.; Chen, C. C.; Jao, M. W. *J. Phys. Chem. B* **2005**, *109*, 9445.
(20) Liu, Z.; Ling, X. Y.; Su, X.; Lee, J. Y. *J. Phys. Chem. B* **2004**, *108*, 8234.
(21) Li, W.; Liang, C.; Zhou, W.; Qiu, J.; Zhou, Z.; Sun, G.; Xin, Q. *J. Phys. Chem. B* **2003**, *107*, 6292.
(22) Park, K. W.; Choi, J. H.; Kwon, B. K.; Lee, S. A.; Sung, Y. E.; Ha, H. Y.; Hong, S. A.; Kim, H. Y.; Wieckowski, A. *J. Phys. Chem. B* **2002**, *106*, 1869.
(23) Adenier, A.; Chehimi, M. M.; Gallardo, I.; Pinson, J.; Vila, N. *Langmuir* **2004**, *20*, 8243.
(24) Hecq, A.; Delrue, J. P.; Hecq, M.; Robert, T. *J. Mater. Sci.* **1981**, *16*, 407.
(25) Sharma, J.; Mahima, S.; Kakade, A. B.; Pasricha, R.; Mandale, A. B.; Vijayamohanan, K. *J. Phys. Chem. B* **2004**, *108*, 13280.
(26) Sharma, J.; Chaki, N. K.; Mandale, A. B.; Pasricha, R.; Vijayamohanan, K. *Electrochim. Acta* **2004**, *272*, 145.
(27) Haimov, A.; Cohen, H.; Neumann, R. *J. Am. Chem. Soc.* **2004**, *126*, 11762.
(28) Liu, Z.; Lee, J. Y.; Chen, W.; Han, M.; Gan, L. M. *Langmuir* **2004**, *20*, 181.
(29) Shukla, A. K.; Neergat, M.; Bera, P.; Jayaram, V.; Hedge, S. M. *J. Electroanal. Chem.* **2001**, *504*, 111.
(30) Prabhuram, J.; Zhao, T. S.; Wong, C. W.; Guo, J. W. *J. Power Sources* **2004**, *134*, 1.
(31) Watanabe, M.; Motto, M. *J. Electroanal. Chem.* **1975**, *60*, 275.
(32) Manohara, R.; Goodenough, J. B. *J. Mater. Chem.* **1992**, *2*, 875.
(33) Liu, Y. C.; Qiu, X. P.; Huang, Y. Q.; Zhu, W. T. *Carbon* **2002**, *40*, 2375.
(34) Frelink, T.; Visscher, W.; van Veen, J. A. R. *J. Electroanal. Chem.* **1995**, *382*, 65.
(35) Peuckert, M.; Yoneda, T.; Dalla Betta, R. A.; Boudart, M. *J. Electrochem. Soc.* **1986**, *113*, 944.